Journal of Solid State Chemistry 182 (2009) 2104–2110

Contents lists available at ScienceDirect

Journal of Solid State Chemistry

journal homepage: www.elsevier.com/locate/jssc

Synthesis and magnetic properties of $ALnO_2$ (A = Cu or Ag; Ln = rare earths) with the delafossite structure

Naoyuki Miyasaka, Yoshihiro Doi, Yukio Hinatsu *

Division of Chemistry, Hokkaido University, Sapporo 060-0810, Japan

ARTICLE INFO

Article history:
Received 22 April 2009
Received in revised form
25 May 2009
Accepted 27 May 2009
Available online 2 June 2009

Keywords:
Magnetic properties
Rare earth
Oxides
Delafossite structure
Magnetic susceptibility

ABSTRACT

Synthesis, structures, and magnetic properties of ternary rare earth oxides $ALnO_2$ (A = Cu or Ag; Ln = rare earths) have been investigated. $CuLnO_2$ (Ln = La, Pr, Nd, Sm, Eu) were synthesized by the direct solid state reaction of Cu_2O and Ln_2O_3, and $AgLnO_2$ (Ln = Tm, Yb, Lu) were obtained by the cation-exchange reaction of $NaLnO_2$ and $AgNO_3$ in a KNO_3 flux. These compounds crystallized in the delafossite-type structure with the rhombohedral 3R type (space group: R-3m). Magnetic susceptibility measurements showed that these compounds are paramagnetic down to 1.8 K. Specific heat measurements down to 0.4 K indicated that $CuNdO_2$ ordered antiferromagnetically at 0.8 K.

1. Introduction

It is well known that oxides containing rare earth elements show a variety of magnetic properties due to the behavior of unpaired 4*f* electrons. When the rare earth ions are arrayed in a structurally characteristic manner, interesting magnetic behavior has been often found. Here, we focus our attention on compounds with the delafossite-type ($CuFeO_2$) structure.

The synthesis, crystal structure, and electric transport properties of delafossite-type compounds were reported by Shannon, Rogers and Prewitt [1–3] and reviewed by Cann et al. [4]. Compounds with this structure have been of immense interest due to the discovery of the p-type transparent conductivity for $CuAlO_2$ [5]. Recently, the optical and electrical properties of silver delafossites were reported [6].

Delafossite compounds belong to a family of ternary oxides with the general formula ABO_2. In this structure, the A cation is linearly coordinated to two oxygen ions and occupied by a noble metal cation in the +1 oxidation state. Typical A cations include Pd, Pt, Cu, or Ag. The B cation is located in distorted edge-shared BO_6 octahedra with a central metal cation having a +3 charge. The delafossite structure can be visualized as consisting of two alternating layers: a planar layer of A cations in a triangular pattern and a layer of edge-sharing BO_6 octahedra flattened with respect to the *c* axis. Depending on the stacking of the double layers (close-packed A cations and BO_6 octahedra), the delafossite structure can form as one of two polytypes, i.e., the hexagonal 2H type and the rhombohedral 3R type.

In this structure, the B cations adopt triangular geometric arrangements. If the magnetic ions are located in the B sites, and if there exists an antiferromagnetic interaction between the nearest-neighbor magnetic ions, they can show magnetic frustrations.

There are some reports on the delafossite-type compounds containing rare earths. Haas et al. reported the preparation of $CuLnO_2$ (Ln = La, Pr, Nd, Sm, and Eu) [7]. Oxygen excess in delafossite structures was reported in the $CuLnO_2$ family, where several researchers have demonstrated the possibility to insert oxygen atoms in the Cu layer, namely in the center of Cu triangles [8–10]. Very recently, the preparation of one silver delafossite-type compound $AgYbO_2$ was reported [11].

In this study, we tried to synthesize a series of $ALnO_2$ (A = Cu or Ag; Ln = rare earths) and determined their crystal structures through the Rietveld analysis for the powder X-ray diffraction data. In these compounds, paramagnetic Ln ions adopt the triangle-based array. Therefore, anomalous magnetic properties reflecting the geometric frustration may be observed. In order to elucidate basic magnetic properties of $ALnO_2$ compounds containing rare earths, their magnetic susceptibilities were measured in the temperature range between 1.8 and 400 K. In addition, specific heat measurements of $CuNdO_2$ were performed in the temperature range between 0.4 and 300 K.

2. Experimental

2.1. Sample preparation

The $CuLnO_2$ (Ln = La, Pr, Nd, Sm, Eu) were prepared by heating 1:1 mixtures of Cu_2O and Ln_2O_3 in a flowing atmosphere of Ar gas

* Corresponding author.
E-mail address: hinatsu@sci.hokudai.ac.jp (Y. Hinatsu).

0022-4596/$ - see front matter © 2009 Elsevier Inc. All rights reserved.
doi:10.1016/j.jssc.2009.05.035

at 1123 K for a day. For La_2O_3 and Nd_2O_3, they absorb moisture in air and easily form lanthanide hydroxides $Ln(OH)_3$. Therefore, these compounds were preheated at 1073 K for a day.

Silver delafossite compounds $AgLnO_2$ were prepared by the following cation-exchange reactions using $NaLnO_2$ as precursors;

$$NaLnO_2+AgNO_3 \rightarrow AgLnO_2+NaNO_3.$$

The reactions were carried out in a flux of $AgNO_3$–KNO_3. The $NaLnO_2$ was prepared by the solid state reactions [12]. As starting materials, Ln_2O_3, Na_2CO_3, and $NaNO_3$ were used. These reagents were weighed in the $Na/Ln = 1.2$ metal ratios to prevent loss of sodium from evaporation, and ground in an agate mortar. The mixtures were pelletized and heated in air at 1173 K for 12–48 h with some addition of Na_2CO_3 or $NaNO_3$ and several regrindings. The obtained $NaLnO_2$ were mixed with $AgNO_3$ and KNO_3 in a dry process (mixing ratio: Na:Ag:K = 3:3:2). The molded samples were heated from 323 to 573 K. After heat treatments, the products were washed with distilled water, ethanol and finally with acetonitrile to eliminate the flux and byproducts.

2.2. X-ray diffraction analysis

Powder X-ray diffraction profiles were measured using a Rigaku Multi-Flex diffractometer with Cu$K\alpha$ radiation equipped with a curved graphite monochromator. The data were collected by step-scanning in the angle range of $10^\circ \le 2\theta \le 120^\circ$ at a 2θ step-size of 0.02°. The X-ray diffraction data were analyzed by the Rietveld technique, using the programs RIETAN2000 [13].

2.3. Magnetic susceptibility measurements

The temperature-dependence of the magnetic susceptibility was measured in an applied field of 0.1 T over the temperature range of $1.8 \le T \le 400$ K, using a SQUID magnetometer (Quantum Design, MPMS5S). The susceptibility measurements were performed under both zero-field-cooled (ZFC) and field-cooled (FC) conditions. The former was measured upon heating the sample to 400 K under the applied magnetic field of 0.1 T after zero-field cooling to 1.8 K. The latter was measured upon cooling the sample from 400 to 1.8 K at 0.1 T.

2.4. Specific heat measurements

The specific heat measurements were carried out using a relaxation technique supplied by the commercial heat capacity measurement system (Quantum Design, Model PPMS). The sample in the form of a pellet (~10 mg) was mounted on an alumina plate with apiezon for better thermal contact. The specific heat and magnetic susceptibility were measured in the temperature range from 0.4 to 300 K.

3. Results and discussion

3.1. Preparation and crystal structure

For A = Cu, we could successfully prepare a series of $CuLnO_2$ compounds with Ln = La, Pr, Nd, Sm, Eu. A representative powder X-ray diffraction profile is shown in Fig. 1 for $CuPrO_2$. The observed diffraction peaks were indexed on a rhombohedral cell with the space group $R\bar{3}m$. The X-ray diffraction data for all the compounds prepared in this study were analyzed by the Rietveld method on the basis of the same space group. The refined structural parameters for $CuPrO_2$ are listed in Table 1. The lattice parameters and reliability factors for all $CuLnO_2$ compounds prepared in this study are summarized in Table 2.

Fig. 2(a) shows a schematic crystal structure of $CuLnO_2$ (Ln = La, Pr, Nd, Sm, Eu). The Ln ions are located in distorted edge-shared LnO_6 octahedra, forming Ln–O layers. The linear O–Cu–O coordination is parallel to the hexagonal c axis. If successive O layers are labeled O1, O2, and O3, the sequence of this structure is (O1 *Ln* O2)–Cu–(O2 *Ln* O3)–Cu–(O3 *Ln* O1)–Cu–O1. This yields a rhombohedral structure with a three-layer periodicity along c axis. The orientation of the LnO_6 octahedra is the same for all layers in this 3R form. This is in contrast with the case for the 2H form in which the orientation of the octahedra switches back and forth [14]. Fig. 2(b) shows a partial projection of the $CuLnO_2$ structure into the hexagonal plane. One layer of LnO_6 octahedra is depicted. As seen from this

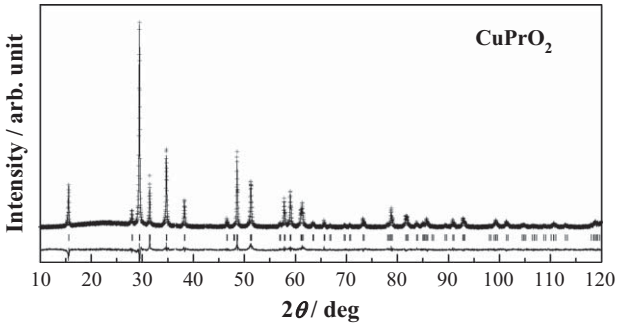

Fig. 1. Powder X-ray diffraction profiles of $CuPrO_2$. The calculated and observed profiles are shown on the top solid line and cross markers, respectively. The vertical marks in the middle show positions calculated for Bragg reflections. The lower trace is a plot of the difference between calculated and observed intensities.

Table 1
Structural parameters for $CuPrO_2$ and $AgLuO_2$.

Atom	Site	x	y	z	B (Å^2)
$CuPrO_2$[a]					
Cu	3*a*	0	0	0	0.3(1)
Pr	3*b*	0	0	1/2	0.3(1)
O	6*c*	0	0	0.1047(5)	1.2(2)
$AgLuO_2$[b]					
Ag	3*a*	0	0	0	0.5(1)
Lu	3*b*	0	0	1/2	0.1(1)
O	6*c*	0	0	0.1074(9)	1.2(2)

[a] *Note*: Space group $R\bar{3}m$, $a = 3.7518(2)$ Å, $c = 17.086(2)$ Å, $R_{wp} = 8.46\%$, $R_I = 8.80\%$, and $R_e = 5.69\%$. Definition of reliability factors R_{wp}, R_I and R_e are given as follows: $R_{wp} = [\sum w(|F(o)| - |F(c)|)^2 / \sum w|F(o)|^2]^{1/2}$, $R_I = \sum |I_k(o) - I_k(c)| / \sum I_k(o)$, and $R_e = [N - p/\sum_i w_i y_i^2]^{1/2}$.

[b] *Note*: Space group $R\bar{3}m$, $a = 3.4086(9)$ Å, $c = 18.588(8)$ Å, $R_{wp} = 14.13\%$, $R_I = 3.17\%$, and $R_e = 4.87\%$.

Table 2
Lattice parameters and reliability factors for $CuLnO_2$ and $AgLnO_2$.

Compounds	a (Å)	c (Å)	R_{wp} (%)	R_I (%)	R_e (%)
$CuLaO_2$	3.8326(2)	17.092(2)	9.14	7.74	5.70
$CuPrO_2$	3.7518(2)	17.086(2)	8.46	8.80	5.69
$CuNdO_2$	3.7119(2)	17.085(2)	7.63	9.27	4.36
$CuSmO_2$	3.6628(1)	17.078(2)	9.38	3.51	6.63
$CuEuO_2$	3.6316(2)	17.074(4)	12.65	8.03	6.18
$AgTmO_2$	3.4670(9)	18.588(12)	14.85	5.02	4.45
$AgYbO_2$	3.4404(11)	18.587(13)	15.68	5.21	4.79
$AgLuO_2$	3.4086(9)	18.588(8)	14.13	3.17	4.87

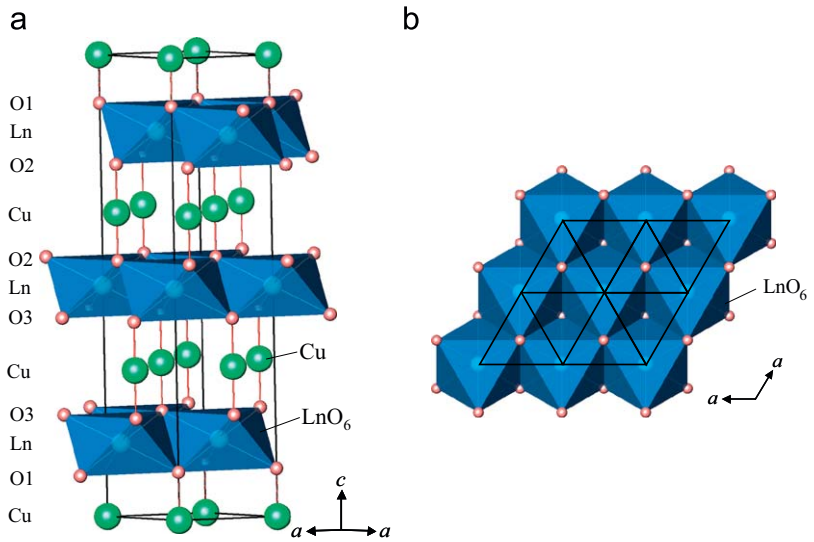

Fig. 2. (a) The schematic crystal structure of CuLnO$_2$; (b) structure of CuLnO$_2$ viewed from the c axis. Only one layer of LnO$_6$ octahedra is shown. The Ln ions form triangular array perpendicular to the c axis (see text).

figure, Ln ions adopt the triangle-based array. Above and below this layer, triangular Cu layers exist.

For A = Ag, a single-phase compound AgLnO$_2$ was prepared for Ln = Tm, Yb, and Lu by the cation-exchange reaction using NaLnO$_2$. The precursors NaLnO$_2$ (Ln = Tm–Lu) adopt the α-NaFeO$_2$ structure (space group: R-3m), and the Ln ion is octahedrally coordinated by six oxygen ions. The crystal structure of AgLnO$_2$ is the same with that of CuLnO$_2$ (Ln = La, Pr, Nd, Sm, Eu). That is, the replacement of sodium by silver in the hexagonal framework brings an important change of the coordination of the interlayer cation. The coordination number decreases from 6 in NaLnO$_2$ to 2 in AgLnO$_2$. The refined positional parameters of AgLuO$_2$ are listed in Table 1, and the lattice parameters for AgLnO$_2$ (Ln = Tm, Yb, Lu) are also summarized in Table 2.

Some bond lengths (A–O, Ln–O) and the bond valence sums (BVSs) [15,16] for Ln and Cu(Ag) ions were calculated using the refined structural parameters, and they are listed in Table 3. The BVS values for the Ln ion are almost constant (~3.0) and they are reasonable for trivalent ions. However, the BVS values of the Ln ions in CuLnO$_2$ are actually increasing with decreasing the ionic radius of Ln^{3+}. It is estimated that for smaller size of Ln ions (Ln = Gd–Lu), the BVS values should be calculated to be much larger than 3. This accounts for the difficulty in preparing the delafossite-type CuLnO$_2$ compounds with the smaller size of Ln ions. Those for the Cu and Ag ions are close to 1.0 for all of the ALnO$_2$ compounds except CuLaO$_2$. The Cu–O bond length of CuLaO$_2$ is a little shorter than the value expected for Cu^+–O^{2-} and the BVS value for the Cu^+ is calculated to be 1.33, which indicates some oxidation of Cu^+ ions. This will be discussed later.

Fig. 3 shows the variation of lattice parameters with the ionic radius of Ln^{3+} for CuLnO$_2$ and AgLnO$_2$. The value of a is strongly influenced by the ionic radii of the Ln ion, while the c value is fixed largely by the O–Cu–O or O–Ag–O bond length. This trend is directly reflected by the structure. Due to the repulsive nature of the Ln^{3+} ions along the shared octahedral edges, a distortion occurs, resulting in a shortened interatomic distance between the oxygen ions. As the Ln ionic radius increases, the Ln–O distance increases while the O–O contact distance remains relatively unchanged. Therefore, an increase in the Ln ionic size has little impact on the c lattice parameter.

We tried to prepare CuLnO$_2$ type compounds for Ln = Ce or Gd–Lu. However, starting materials did not react even at higher temperatures than 1200 K. For cerium compounds, this is due to the fact that the Ce^{4+} ion is more stable than Ce^{3+}. For the case of Ln = Gd–Lu, the atomic distance between Cu should become too smaller, because the a axis lattice parameter decreases with decreasing Ln^{3+} ionic size. The strong electric repulsion between Cu^+ will make difficult to form CuLnO$_2$ compounds.

Table 3
Bond lengths and BVSs for ALnO$_2$ (A = Cu, Ag).

Compounds	d(A–O) (Å)	BVS	d(Ln–O) (Å)	BVS
CuLaO$_2$	1.760(9) × 2	1.33	2.466(4) × 6	2.71
CuPrO$_2$	1.789(8) × 2	1.23	2.411(4) × 6	2.85
CuNdO$_2$	1.836(7) × 2	1.09	2.370(3) × 6	3.03
CuSmO$_2$	1.880(8) × 2	0.96	2.325(3) × 6	3.16
CuEuO$_2$	1.895(9) × 2	0.93	2.302(5) × 6	3.26
AgTmO$_2$	2.017(11) × 2	1.13	2.275(8) × 6	2.85
AgYbO$_2$	2.034(12) × 2	1.08	2.253(7) × 6	2.78
AgLuO$_2$	1.996(9) × 2	1.19	2.256(3) × 6	2.91

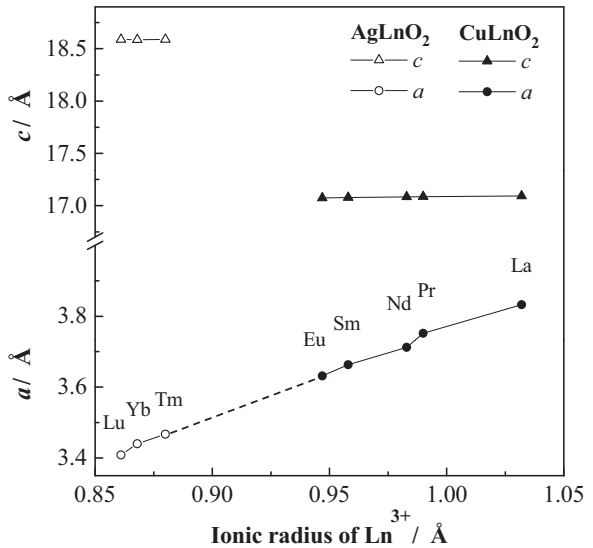

Fig. 3. Variation of lattice parameters for CuLnO$_2$ and AgLnO$_2$ with the ionic radius of Ln^{3+}.

3.3. Magnetic properties

The results of the magnetic susceptibility measurements on Cu*Ln*O_2 (*Ln* = La, Pr, Nd, Sm, Eu) and Ag*Ln*O_2 (*Ln* = Tm, Yb, Lu) are summarized in Table 4. Compounds Cu*Ln*O_2 (*Ln* = Pr, Nd, Sm, Eu) and Ag*Ln*O_2 (*Ln* = Tm, Yb) are paramagnetic in the temperature range between 1.8 and 400 K. Even a lanthanum-containing compound $CuLaO_2$ shows paramagnetic behavior. Magnetic properties of each compound will hereinafter be described.

3.3.1. $CuLnO_2$ (*Ln* = La, Pr, Nd, Sm, Eu)

Fig. 4 shows the magnetic susceptibility–temperature curve of $CuLaO_2$. This temperature dependence of the susceptibility indicates the existence of paramagnetic substance in the $CuLaO_2$ compound. If the oxygen-stoichiometric compounds were formed, there should exist no magnetic ions. Experimental results indicate that some Cu^+ ions are oxidized to the divalent state due to the existence of excess oxygen ions. It is known that excess oxygen in the delafossite structure was reported in the Cu*Ln*O_2 compounds [8–10], where several researchers demonstrated the possibility to insert oxygen atoms in the Cu layers [10].

The temperature dependence of the magnetic susceptibility of $CuLaO_2$ prepared in this study (actually $CuLaO_{2+\delta}$) can be fitted by the Curie law including the temperature independent term,

$$\chi = C/T + \chi_{TIP},$$

and the effective magnetic moment is obtained to be $\mu_{eff} = 0.264\ \mu_B$ per $CuLaO_{2+\delta}$. Since the effective magnetic moment of Cu^{2+} with $[Ar]3d^9$ electronic configuration is 1.73 μ_B, the ratio of the Cu^{2+}/Cu is estimated to be $(0.264/1.73)^2 = 0.024$. Therefore, the oxygen-nonstoichiometry of $CuLaO_{2+\delta}$ is $\delta = 0.012$. This value is very close to that for the $CuLaO_{2.01}$ sample prepared under the same conditions [9].

Figs. 5 and 6 show the temperature dependences of the magnetic susceptibility of $CuPrO_2$ and $CuNdO_2$, respectively. Both of them indicate no magnetic transition in the temperature range between 1.8 and 400 K, and the susceptibilities follow the Curie–Weiss law. The obtained effective magnetic moment and the Weiss constant are listed in Table 4. The effective magnetic moments of these compounds are almost equal to those of the free ion value of Ln^{3+}. However, the effective magnetic moment of $CuPrO_2$ is actually a bit of larger than the moment of Pr^{3+} ion. This

Table 4
Effective magnetic moments (μ_{eff}: experimental, $\mu_{Ln^{3+}}$: calculated) and Weiss constants for Cu*Ln*O_2 and Ag*Ln*O_2.

Compounds	μ_{eff} (μ_B)	$\mu_{Ln^{3+}}$ (μ_B)	θ (K)	θ_{LT} (K)[a]	
$CuLaO_2$	0.26(1)	–	–	–	para. (>1.8 K)
$CuPrO_2$	3.75(6)	3.58	−113(6)	–	para. (>1.8 K)
$CuNdO_2$	3.55(1)	3.62	−50(1)	−3.79(6)	AF (T_N = 0.8 K)
$CuSmO_2$	1.66(1)[b]	1.55[c]	–	–	van Vleck
$CuEuO_2$	3.53(1)[b]	3.40[c]	–	–	van Vleck
$AgTmO_2$	7.52(1)	7.55	−34(1)	–	para. (>1.8 K)
$AgYbO_2$	4.46(1)	4.54	−66(2)	−2.98(2)	para. (>1.8 K)
$AgLuO_2$	–	–	–	–	dia.

Note: para: paramagnetic, AF: antiferromagnetic, dia: diamagnetic.

[a] Weiss constants obtained from low temperature data (<10 K).
[b] Observed values at room temperature.
[c] Calculated values by van Vleck [19].

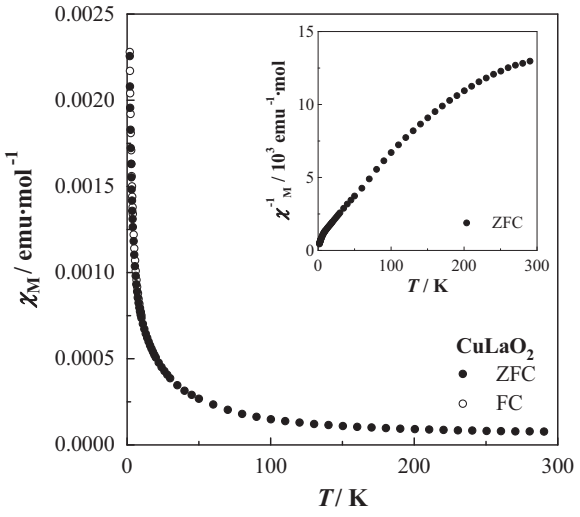

Fig. 4. Temperature dependence of the magnetic susceptibility of $CuLaO_2$. The inset shows the reciprocal susceptibility vs. temperature curve.

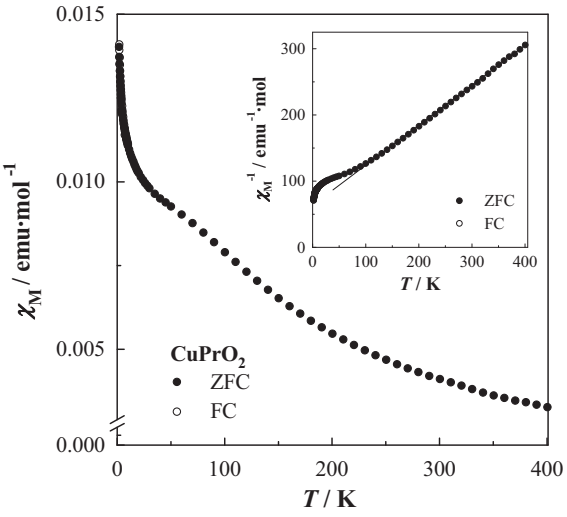

Fig. 5. Temperature dependence of the magnetic susceptibility of $CuPrO_2$. The inset shows the reciprocal susceptibility vs. temperature curve. The solid line is the Curie–Weiss fitting.

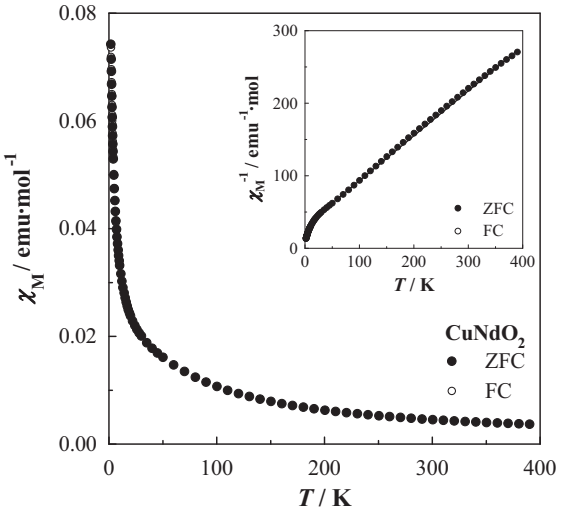

Fig. 6. Temperature dependence of the magnetic susceptibility of $CuNdO_2$. The inset shows the reciprocal susceptibility vs. temperature curve. The solid line is the Curie–Weiss fitting.

is due to the existence of some Cu^{2+} ions in $CuPrO_2$. The Pr^{3+} ion is located in a distorted LnO_6 octahedron. The ground state $^3H_4$ of the Pr^{3+} ion is split into one singlet (Γ_1), one doublet (Γ_3), and two triplets (Γ_4 and Γ_5) in the octahedral symmetry [17]. We expect that the ground state and the first excited state are Γ_1 and Γ_4, respectively, and that the upper excited states are Γ_3 and Γ_5. In that case, the magnetic susceptibility of the Pr^{3+} ion should be temperature-independent at low temperatures (for example, in the temperature region below 50 K) [18]. The rapid increase of the magnetic susceptibility of $CuPrO_2$ with decreasing temperature also shows the existence of Cu^{2+} ions in $CuPrO_2$. The large deviation of the magnetic susceptibility from the Curie–Weiss law around 50 K is ascribed to the paramagnetic behavior of Cu^{2+} ions. The negative Weiss constants suggest the existence of antiferromagnetic interaction at lower temperatures. However, the Weiss constants obtained from high temperature (50–400 K) data are obviously overestimated due to the crystal field splitting of the ground state of Ln^{3+} ions. In order to assess them, the Weiss constant at low temperature (θ_{LT}) was also calculated from the data between 1.8 and 15 K for $CuNdO_2$. The negative value of θ_{LT} (-3.79 K) indicates that if we perform magnetic susceptibility measurements at furthermore lower temperatures, the antiferromagnetic interaction should be observed. Specific heat measurements for $CuNdO_2$ down to 0.4 K showed the antiferromagnetic interaction between Nd^{3+} ions, which will be described later section.

Magnetic susceptibilities of $CuSmO_2$ and $CuEuO_2$ are plotted as a function of temperature in Fig. 7. No magnetic transition was observed down to 1.8 K. Both the magnetic susceptibilities do not obey the Curie–Weiss law. For the Sm^{3+} and Eu^{3+} ions, the multiplet levels are not large compared to k_BT (k_B: Boltzmann constant), so the excited state should contribute to the magnetic susceptibility. A susceptibility plateau of $CuEuO_2$ is observed below 50 K, which is attributed to the temperature-independent term of the Van Vleck formula [19]. Since the ground state of Eu^{3+} ion is $^7F_0$, i.e., nonmagnetic, the Eu^{3+} ion does not contribute to the temperature dependence of the magnetic susceptibility at low temperatures ($T<50$ K). The increase of the magnetic susceptibility below 20 K is due to the presence of some Cu^{2+} ions in this $EuCuO_2$ as in the case of $LaCuO_2$. The effective magnetic moments (μ_{eff}) of $CuSmO_2$ and $CuEuO_2$ are estimated from the data only at room temperature. The μ_{eff} values are very close to the moments calculated for free Ln^{3+} ions (see Table 4).

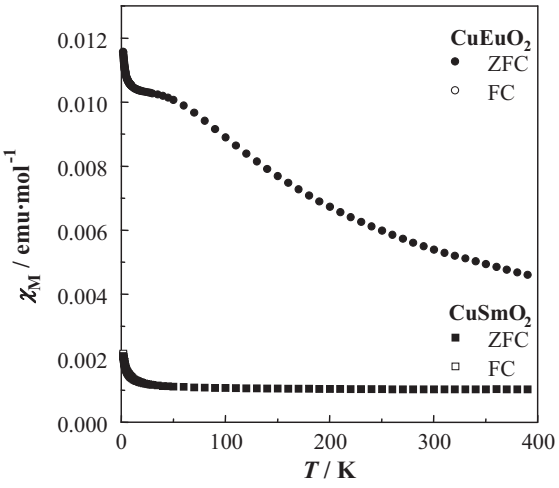

Fig. 7. Temperature dependence of the magnetic susceptibility of $CuSmO_2$ and $CuEuO_2$.

3.3.2. $AgLnO_2$ ($Ln = Tm$, Yb)

Fig. 8 shows the temperature dependence of the magnetic susceptibility of $AgTmO_2$ in the temperature range between 1.8 and 300 K. No magnetic anomaly was observed down to 1.8 K and this compound shows paramagnetic behavior in this temperature range. The inset of Fig. 8 depicts the reciprocal susceptibility against temperature. The Curie–Weiss fitting in the temperature range between 100 and 300 K gives the effective magnetic moment of 7.52 μ_B. This value is almost consistent with the theoretical moment for Tm^{3+} (7.55 μ_B), indicating that the thulium ion is in the trivalent state.

Similar magnetic results have been observed for the magnetic susceptibility of $AgYbO_2$. Fig. 9 depicts its magnetic susceptibility vs. temperature curve and the inset shows the temperature dependence of the reciprocal susceptibility. This compound also shows paramagnetic behavior in the temperature range between

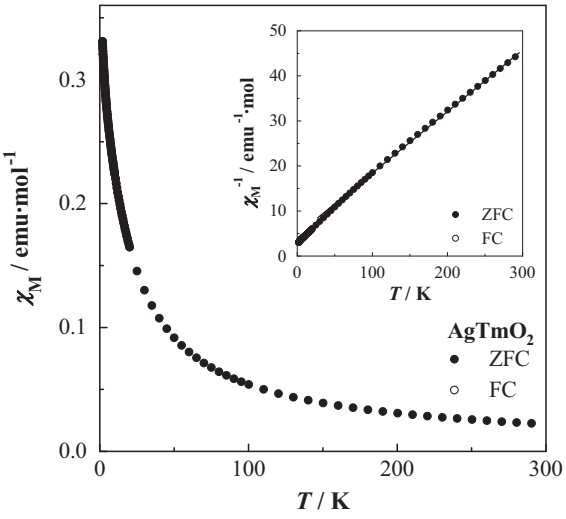

Fig. 8. Temperature dependence of the magnetic susceptibility of $AgTmO_2$. The inset shows the reciprocal susceptibility vs. temperature curve. The solid line is the Curie–Weiss fitting.

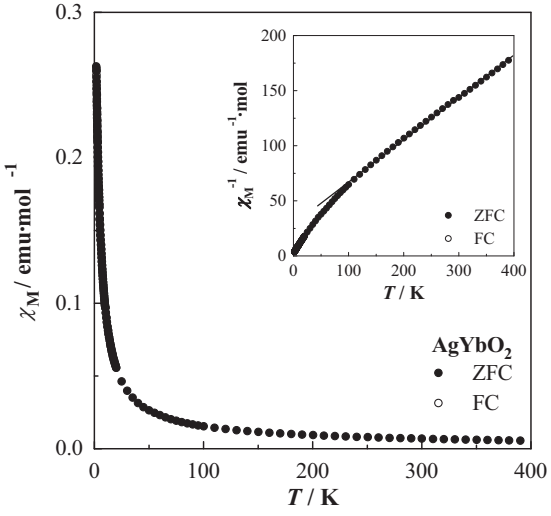

Fig. 9. Temperature dependence of the magnetic susceptibility of $AgYbO_2$. The inset shows the reciprocal susceptibility vs. temperature curve. The solid line is the Curie–Weiss fitting.

1.8 and 400 K. The Curie–Weiss fitting in the temperature range between 100 and 400 K gives the effective magnetic moment of 4.46 μ_B. This value is close to the theoretical moment for Yb^{3+} (4.54 μ_B), indicating that the ytterbium ion is in the trivalent state. The negative Weiss constant $\theta = -66$ K suggests the existence of antiferromagnetic interaction. The Weiss constant in a low-temperature region from 1.8 to 20 K (θ_{LT}) was also calculated to prevent its overestimation by the convexity of the reciprocal susceptibility vs. temperature curve due to the crystal field effect. It is $\theta_{LT} = -2.98$ K, indicating that the antiferromagnetic interaction should be observed at furthermore lower temperatures.

3.3.3. Specific heat results for $CuNdO_2$

For $CuNdO_2$, specific heat measurements were performed in the temperature range between 0.4 and 300 K. Fig. 10(a) shows the temperature dependence of the specific heat C_p for $CuNdO_2$ between 0.4 and 15 K. The specific heat data show a λ-type anomaly at 0.8 K, indicating the existence of the long-range magnetic ordering. To calculate the magnetic contribution to the specific heat, we have to subtract the contribution of lattice specific heat from the total specific heat. They were estimated by using a polynomial function of the temperature, $f(T) = aT^3+bT^5+cT^7$ [20], in which the constants a, b and c were determined by fitting this function to the observed specific heat data above 10 K. Fig. 10(b) shows the temperature dependence of the magnetic specific heat divided by temperature (C_{mag}/T). From the temperature dependence of the magnetic specific heat, the magnetic entropy change of $CuNdO_2$ is calculated by the relation $S_{mag} = \int (C_{mag}/T)\, dT$. It is also shown in Fig. 10(b). The magnetic entropy change due to the antiferromagnetic ordering is determined to be 5.8 J mol^{-1} K^{-1}.

In an octahedral crystal field environment, the ground state of the Nd^{3+} ion (the electronic configuration: [Xe]$4f^3$, the state $^4I_{9/2}$) is the ten-fold degenerate state. The magnetic entropy change of Nd^{3+} is calculated to be $R\ln(2J+1) = R\ln 10 = 19.14$ J mol^{-1} K^{-1}, where R and J are the molar gas constant and the total quantum number, respectively. In the case of lower symmetry, this state splits into five Kramers doublet states. For such a case, the magnetic entropy change is expected to be $R\ln 2 = 5.76$ J mol^{-1} K^{-1}; the experimental value is close to this value. The result of the magnetic entropy change indicates that the degeneracy of the ground state for the Nd^{3+} ion in $CuNdO_2$ should be doublet; the observed magnetic entropy of $R\ln 2$ indicates that the ground doublet is selectively populated at low temperatures and this state causes the antiferromagnetic transition.

The $CuLnO_2$ compounds have a triangle-based array of Ln^{3+} ions and are expected to behave as frustrated magnets. Geometrically frustrated materials often show a large ratio θ/T_m for the Weiss constant (θ) and the magnetic ordering temperature (T_m), since such a frustration suppresses the long-range magnetic ordering [21]. In the case of $CuNdO_2$, the θ_{LT}/T_m value is 5. This result indicates that the magnetic ordering is highly suppressed by the magnetic frustration, that is, the magnetic interaction between Ln ions in the Ln–O layers should be frustrated. Further studies such as neutron diffraction measurements will elucidate whether the magnetic frustration due to the triangular lattice is operative in the whole temperature range.

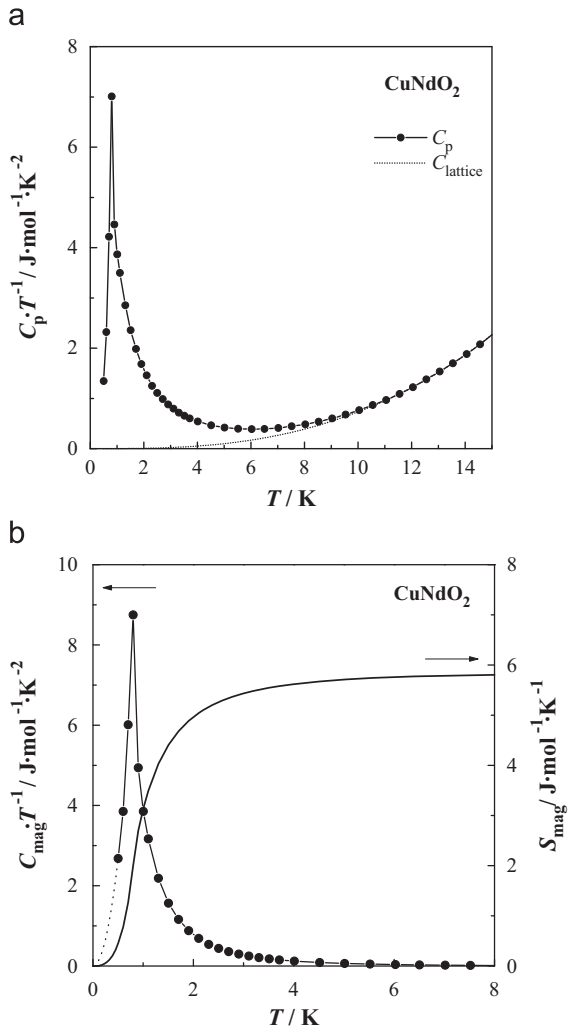

Fig. 10. (a) Temperature dependence of the specific heat C_p for $CuNdO_2$ below 15 K. The dotted line is the calculation results for the lattice specific heat (see text); (b) temperature dependences of the magnetic specific heat divided by temperature C_{mag}/T and the magnetic entropy change S_{mag} for $CuNdO_2$ below 8 K.

Acknowledgement

This work was supported by Grant-in-aid for Scientific Research, No. 20550052 from the Ministry of Education, Science, Sports, and Culture of Japan.

References

[1] R.D. Shannon, D.B. Rogers, C.T. Prewitt, Inorg. Chem. 10 (1971) 713–718.
[2] C.T. Prewitt, R.D. Shannon, D.B. Rogers, Inorg. Chem. 10 (1971) 719–723.
[3] D.B. Rogers, R.D. Shannon, C.T. Prewitt, J.L. Gillson, Inorg. Chem. 10 (1971) 723–727.
[4] M.A. Marquardt, N.A. Ashmore, D.P. Cann, Thin Solid Films 496 (2006) 146–156.
[5] H. Kawazoe, M. Yasukawa, H. Hyodo, M. Kurita, H. Yanagi, H. Hosono, Nature 389 (1997) 939–942.
[6] W.C. Sheets, E.S. Stampler, M.I. Bertoni, M. Sasaki, T.J. Marks, T.O. Mason, K.R. Poeppelmeier, Inorg. Chem. 47 (2008) 2696–2705.
[7] H. Haas, E.Z. Kordes, Kristallografiya 129 (1969) 259–270.
[8] R.J. Cava, H.W. Zandbergen, A.P. Ramirez, H. Takagi, C.T. Chen, J.J. Krajewski, W.F. Peck Jr., J.V. Waszczak, G. Meigs., R.S. Roth, L.F. Schneemeyer, J. Solid State Chem. 104 (1993) 427–452.
[9] M. Trari, J. Topfer, J.P. Doumerc, M. Pouchard, A. Ammar, P. Hagenmuller, J. Solid State Chem. 111 (1994) 104–110.
[10] K. Isawa, Y. Yaegashi, M. Komatsu, M. Nagano, S. Sudo, M. Karppinen, H. Yamauchi, Phys. Rev. B 56 (1997) 3457–3466.
[11] A. Saito, N. Sawaguchi, M. Sasaki, J. Ceramic Soc. Japan 116 (2008) 118–120.
[12] Y. Hashimoto, M. Wakeshima, Y. Hinatsu, J. Solid State Chem. 176 (2003) 266–272.
[13] F. Izumi, T. Ikeda, Mater. Sci. Forum 198 (2000) 321–324.
[14] J. Li, A.F.T. Yokochi, A.W. Sleight, Solid State Sci. 6 (2004) 831–839.

[15] I.D. Brown, A. Altermatt, Acta Crystallogr. Sect. B 41 (1985) 244–247.
[16] N.E. Brese, M. O'Keeffe, Acta. Crystallogr. Sect. B 47 (1991) 192–197.
[17] K.R. Lea, N.J.M. Leask, W.P. Wolf, J. Phys. Chem. Solids 23 (1962) 1381–1395.
[18] Y. Doi, Y. Hinatsu, J. Phys. Condens. Matter 13 (2001) 4191–4202.
[19] J.H. van Vleck, The Theory of Electric and Magnetic Susceptibilities, Clarendon, Oxford, 1932.
[20] J.E. Gordon, R.A. Fisher, Y.X. Jia, N.E. Phillips, S.F. Reklis, D.A. Wright, A. Zettl, Phys. Rev. B 59 (1999) 127–130.
[21] J.E. Greedan, J. Mater. Chem. 11 (2001) 37–53.